

PROBING THE COMPLEX AND VARIABLE X-RAY ABSORPTION OF MARKARIAN 6 WITH
XMM-NEWTON

STEFAN IMMLER,¹ W. N. BRANDT,¹ CRISTIAN VIGNALI,¹ FRANZ E. BAUER,¹
D. MICHAEL CRENSHAW,² JOHN J. FELDMEIER,³ AND STEVEN B. KRAEMER⁴
Draft version November 4, 2018

ABSTRACT

We report on an X-ray observation of the Seyfert 1.5 galaxy Mrk 6 obtained with the EPIC instruments onboard *XMM-Newton*. Archival *BeppoSAX* PDS data from 18–120 keV were also used to constrain the underlying hard power-law continuum. The results from our spectral analyses generally favor a double partial-covering model, although other spectral models such as absorption by a mixture of partially ionized and neutral gas cannot be firmly ruled out. Our best-fitting model consists of a power law with a photon index of $\Gamma = 1.81^{+0.22}_{-0.20}$ and partial covering with large column densities up to $N_{\text{H}} \sim 10^{23} \text{ cm}^{-2}$. We also detect a narrow emission line consistent with Fe K α fluorescence at $6.45^{+0.03}_{-0.04} \text{ keV}$ with an equivalent width of $93^{+26}_{-20} \text{ eV}$. Joint analyses of *XMM-Newton*, *ASCA*, and *BeppoSAX* data further provide evidence for both spectral variability (a factor of ~ 2 change in absorbing column) and absorption-corrected flux variations (by $\sim 60\%$) during the ~ 4 year period probed by the observations.

Subject headings: galaxies: individual (Mrk 6) — galaxies: Seyfert — X-rays: galaxies

1. INTRODUCTION

Markarian 6 (Mrk 6, IC 0450; $z = 0.0188$; 77 Mpc distant for $H_0 = 75 \text{ km s}^{-1} \text{ Mpc}^{-1}$) is one of a handful of intermediate Seyferts of type 1.5, including NGC 4151 and Mrk 766, showing evidence for an ‘ionization cone’ rather than the ‘ionization halo’ expected for a type 1 viewing geometry (Meaburn, Whitehead, & Pedlar 1989; Kukulka et al. 1996). A torus ‘atmosphere’ along the line of sight has been suggested to explain the presence of the ionization cone (e.g., Evans et al. 1993). The torus atmosphere is thought to be optically thick for ionizing radiation between the Lyman edge and soft X-rays, but it allows radiation outside of this spectral range (e.g., broad optical line emission from the Broad Line Region) to pass through with only moderate obscuration. Mrk 6 shows significant optical line profile variations on time-scales of months to years, suggesting that at least some of the gaseous material creating the lines can undergo coherent variations (e.g., Rosenblatt et al. 1992; Eracleous & Halpern 1993).

X-ray investigations of Seyfert galaxies are well suited to probing matter along the line of sight toward their central black hole regions. Prominent examples of intermediate Seyferts that have been well studied in X-rays include the ‘cousins’ of Mrk 6, NGC 4151 (e.g., Weaver et al. 1994; Ogle et al. 2000; Yang, Wilson, & Ferruit 2001; Schurch & Warwick 2002) and Mrk 766 (e.g., Leighly et al. 1996; Page et al. 1999, 2001; Matt et al. 2000; Branduardi-Raymont et al. 2001). In contrast, the only published X-ray study of Mrk 6 is that of Feldmeier et al. (1999; hereafter F99) using 0.6–9.5 keV *ASCA* data. These data revealed heavy and complex X-ray absorption that was best fit by a double partial-covering model with large column densities [$\sim (3-$

$20) \times 10^{22} \text{ cm}^{-2}$], likely due to the torus atmosphere. However, detailed X-ray spectral modeling was limited by modest photon statistics and the fact that the absorption in Mrk 6 dominates the X-ray spectrum throughout most of the *ASCA* bandpass.

We capitalized on the superior throughput (about an order of magnitude higher than *ASCA*) and good spectral resolution of the instruments onboard *XMM-Newton* to investigate further the X-ray emission and absorption properties of Mrk 6. We also used the *XMM-Newton* data to perform sensitive searches for temporal and spectral variability during the observation and in comparison with earlier *ASCA* and *BeppoSAX* observations.

2. X-RAY OBSERVATIONS AND DATA REDUCTION

2.1. *XMM-Newton*

Mrk 6 was observed with the European Photon Imaging Camera (EPIC) onboard *XMM-Newton* (Jansen et al. 2001) with on-source exposure times of 31.8 ks (EPIC p-n) and 30.8 ks (EPIC MOS 1 and MOS 2). It was also observed with the Reflection Grating Spectrometer (RGS) for 46.4 ks (RGS 1) and 37.9 ks (RGS 2). The EPIC data allow sensitive 0.2–12 keV imaging spectroscopy with moderate spectral ($E/\Delta E \sim 20$ –50) and angular ($6''$ FWHM) resolution. The parameters of the individual observations are listed in Tab. 1.

Both the p-n and MOS data were acquired in ‘full-frame mode’ using the medium filter. The data were reduced using the Science Analysis System (SAS) v5.3.3 with the latest calibration products. Due to background flares at the end of the observation period, 7% of the p-n and 31% of the MOS 1 and MOS 2 data were rejected. After inspection of a source-free background spectrum extracted from

¹ Department of Astronomy & Astrophysics, 525 Davey Laboratory, The Pennsylvania State University, University Park, PA 16802

² Department of Physics and Astronomy, Georgia State University, Atlanta, GA 30303

³ Department of Astronomy, Case Western Reserve University, 10900 Euclid Avenue, Cleveland, OH 44106

⁴ Catholic University of America and Laboratory for Astronomy and Solar Physics, NASA’s Goddard Space Flight Center, Code 681, Greenbelt, MD, 20771

CCD 1 on the p-n and MOS detectors, we selected data only in the 0.3–12 keV energy range due to enhanced background at low photon energies (up to a factor of ~ 5). We furthermore excluded bad and hot pixels from the data. Since the cleaned RGS data did not yield enough photon statistics for spectral analysis, they were not used further.

Source counts were extracted for the p-n and MOS detectors within 30''-radius circular regions (the 85% encircled-energy radius at 7.5 keV). The background was extracted locally from source-free regions. For the p-n we used a rectangular region of size $2'4 \times 3'8$ close to Mrk 6 on the same p-n chip, and for the MOS we used an annulus with inner and outer radii of $2'5$ and $4'3$. Given the observed count rates of ~ 1.2 and ~ 0.4 cts s^{-1} for the p-n and MOS detectors, the pile-up fractions and dead times are estimated to be $\lesssim 2\%$. The source counts were binned with a minimum of 50 counts per bin to allow χ^2 spectral fitting. We also constructed background-corrected light curves of Mrk 6 in the soft (0.3–2 keV), hard (2–12 keV), and broad (0.3–12 keV) bands by binning the events into 250 s intervals and excluding telemetry dropouts.

2.2. *BeppoSAX*

Archival *BeppoSAX* MECS 2+3 (Medium Energy Concentrator Spectrometer) and LECS (Low Energy Concentrator Spectrometer) data are also used in the analyses below (see Tab. 1); these data cover the 1.3–10 keV (MECS) and 0.5–4.5 keV (LECS) energy bands. To extend the spectral range of our analyses to higher photon energies, which is useful to constrain the underlying power-law continuum, we furthermore used the *BeppoSAX* PDS (Phoswich Detection System) data in the energy range 18–120 keV.

We checked for contamination of the PDS data due to other X-ray sources within its field of view ($1'3$ FWHM). No strong X-ray source other than Mrk 6 is found within the $\sim 30'$ -diameter EPIC field of view in high-energy (> 5 keV) images. The *ROSAT* All-Sky Survey broadband source catalog shows only two other X-ray sources (NGC 2256 and NGC 2258) located within the PDS field of view at large off-axis angles ($23'2$ and $18'1$). Both of these sources have 2–10 keV MECS fluxes much lower (only ~ 2 –3%) than that of Mrk 6. Since the PDS effective area decreases sharply with increasing off-axis angle, their contamination to the Mrk 6 PDS spectrum is negligible.

3. RESULTS

3.1. *Spectral Analysis*

Spectral analysis was performed using XSPEC v11.2 (Arnaud 1996). All errors are quoted at the 90% level of confidence for one parameter of interest ($\Delta\chi^2 = 2.71$; Avni 1976) and Galactic absorption ($N_{\text{H}} = 6.4 \times 10^{20}$ cm^{-2} ; Stark et al. 1992) is always implicitly included. The previous *ASCA* observation has shown that Mrk 6 is an intrinsically absorbed system ($\gtrsim 10^{22}$ – 10^{23} cm^{-2} ; F99). We therefore used the 18–120 keV *BeppoSAX* PDS data, which should be much less affected by absorption, to determine the shape of the underlying X-ray continuum. Fitting a power-law model to the PDS data (model 1 in Tab. 2) gives a best-fit photon index of $\Gamma = 1.81^{+0.22}_{-0.20}$ and an unabsorbed 20–100 keV flux of 5.0×10^{-11} ergs cm^{-2} s^{-1} .

We then fitted the *XMM-Newton* and *BeppoSAX* PDS spectra simultaneously. Due to uncertainties in the cross-calibration of the instruments (p-n and MOS: $\lesssim 7\%$; Snowden 2002) as well as possible variability between the *XMM-Newton* and *BeppoSAX* observations, we left all normalizations for the spectral components free. All other spectral parameters were tied together. We first tried fitting a power-law model with simple (fully covering) intrinsic absorption. Such absorption could arise in the host galaxy, perhaps in gas associated with the irregularly distributed dust seen in the *HST* image of Malkan, Gorjian, & Tam (1998). It could also arise on smaller scales in the nuclear region. This model is statistically rejected ($\chi^2_{\nu} = 3.24$; d.o.f. = 867). It also gives a photon index ($\Gamma \sim 0.9$) well below that derived from our *BeppoSAX* PDS analysis and expected intrinsically for a Seyfert galaxy ($\Gamma \sim 1.6$ – 2.2 ; e.g., Nandra et al. 1997; Risaliti 2002).

We next tried fitting a power-law model with a single partial-covering absorption component. Partially covering absorption could arise from electron scattering of X-rays in the nucleus of Mrk 6 (see F99), and such absorption has been used successfully to explain the X-ray spectra of other intermediate Seyferts. This model also includes the simple intrinsic absorption used in the previous model, since again there could be absorption in the host galaxy after the X-rays have escaped the nucleus (this simple intrinsic absorption will be implicitly included in all of the following spectral fits). Finally, we added a Gaussian emission line to model Fe $K\alpha$ emission visible in the spectrum. This model is marginally acceptable ($\chi^2_{\nu} = 1.08$; d.o.f. = 859) although it leaves clear systematic residuals below ~ 2 keV and above ~ 40 keV. Furthermore, like the previous model, it requires an implausibly low photon index of $\Gamma \sim 1.3$. If we constrain the photon index to lie in the range 1.6–2.2, the fit is statistically unacceptable.

Given the failures of the two previous spectral models, we tried a model consisting of a power law and two partially covering absorbers (model 2 in Tab. 2). This model was successfully used by F99 to describe the *ASCA* data, and double partial covering could arise if electron scattering of X-rays provides several lines of sight into the nucleus. The photon index was fixed to the best-fit value derived from the *BeppoSAX* PDS data ($\Gamma = 1.81$; our results are not changed materially if the photon index is left as a free parameter), and we also included a Gaussian Fe $K\alpha$ emission line. Despite some small systematic residuals below ~ 2 keV, a good overall fit to the *XMM-Newton* and *BeppoSAX* data is found ($\chi^2_{\nu} = 0.96$; d.o.f. = 858; see Fig. 1). The absorption includes a high column density ($10.96^{+0.58}_{-0.42} \times 10^{22}$ cm^{-2}) component covering (57 ± 1)% of the emitting region, as well as a lower column density ($2.46^{+0.07}_{-0.05} \times 10^{22}$ cm^{-2}) component with a higher covering percentage of (93 ± 1)%. The best-fit rest-frame energy of the Fe $K\alpha$ line is $6.45^{+0.03}_{-0.04}$ keV with an equivalent width of 93^{+26}_{-20} eV. There is no clear evidence for a broad Fe $K\alpha$ line, and the fitted line properties are consistent with those from *ASCA*. Given its properties, the observed line could originate via reprocessing in the outer part of the accretion disk (e.g., George & Fabian 1991) or perhaps in Broad Line Region clouds (see equation 5 in Eracleous, Halpern, & Livio 1996).

The Fe K α line is fairly weak for a Seyfert galaxy, suggesting that Compton reflection is unlikely to make a dominant contribution to the X-ray spectrum. To examine any effects of Compton reflection further, we replaced the simple power law in the previous fit with a power law plus neutral reflection (the ‘PEXRAV’ model in XSPEC assuming solar abundances). All other aspects of the model were unchanged. We obtain a relative reflection fraction (defined as $r = \Omega/2\pi$, where Ω is the angle subtended by the reflector) of $r = 1.21^{+0.14}_{-0.16}$, an inclination angle of $\cos i = 0.94^{+0.01}_{-0.25}$, and a cut-off energy of ~ 238 keV (model 3 in Tab. 2). The fit quality is slightly improved compared to the previous fit ($\chi^2_\nu = 0.95$; d.o.f. = 855), but there is no material change in the nature of the partially covering absorption. Due to both statistical and systematic uncertainties associated with this model, we do not consider the derived inclination angle to have clear physical significance.

We also tested a model which assumes that the nuclear X-ray emission is attenuated by both partially ionized and neutral material, dispersed along the line of sight. This model was proposed by Schurch & Warwick (2002) to characterize the complex X-ray absorption of NGC 4151, a Seyfert with many similarities to Mrk 6 (see §1). Although the model gives a relatively good fit to the 2–120 keV data, large residuals are visible below ~ 2 keV ($\chi^2_\nu = 1.14$; d.o.f. = 866; see Fig. 1). We obtain an ionization parameter of $\log \xi = \log(L_{\text{ion}}/nr^2) = 2.42 \pm 0.01$ (with L_{ion} the source ionizing luminosity in the 0.0136–13.6 keV band, n the number of hydrogen atoms/ions per cm^{-3} , and r the distance from the central source to the photoionized region), an ionized column density of $1.33^{+0.01}_{-0.02} \times 10^{23} \text{ cm}^{-2}$, and a neutral column density of $3.35^{+0.17}_{-0.11} \times 10^{21} \text{ cm}^{-2}$.

A slightly better fit ($\chi^2_\nu = 1.09$; d.o.f. = 863) is obtained if the simple power law in the previous fit is replaced with a power law plus neutral reflection (model 4 in Tab. 2). As for the double partial-covering model, the reflection is not a dominant spectral component and the best-fit absorption parameters do not change materially.

We performed several additional fits to check the general robustness of our results. Models with no intrinsic absorption and Compton reflection cannot provide acceptable fits. Models with fully covering intrinsic absorption and Compton reflection can at best provide marginally acceptable fits. These models also suffer from physical consistency problems since the energy region near the Fe K α line is dominated by the reflection component. An Fe K α line with a large equivalent width of ~ 1 –2 keV is then expected (e.g., Matt, Brandt, & Fabian 1996) but not observed.

Using the double partial-covering model (model 2 in Tab. 2), we derive observed 0.3–2 keV and 2–10 keV *XMM-Newton* fluxes of $5.3 \times 10^{-13} \text{ ergs cm}^{-2} \text{ s}^{-1}$ and $1.2 \times 10^{-11} \text{ ergs cm}^{-2} \text{ s}^{-1}$, respectively. These values are consistent with those in §2.3.5 of F99, given statistical and systematic uncertainties. The absorption-corrected 2–10 keV flux and luminosity are $2.0 \times 10^{-11} \text{ ergs cm}^{-2} \text{ s}^{-1}$ and $1.4 \times 10^{43} \text{ ergs s}^{-1}$, respectively. The absorption-corrected 0.3–2 keV flux and luminosity are less certain due to the large required absorption correction; likely values are

$\sim 1.5 \times 10^{-11} \text{ ergs cm}^{-2} \text{ s}^{-1}$ and $\sim 1.1 \times 10^{43} \text{ ergs s}^{-1}$, respectively. Using the partially ionized and neutral absorption model (model 4 in Tab. 2), we derive an absorption-corrected 2–10 keV flux and luminosity $\sim 36\%$ lower than from the double partial-covering model.

3.2. Temporal and Spectral Variability

After fitting constant models to light curves and inspecting the residuals, we do not find any rapid, large-amplitude X-ray variability during the *XMM-Newton* or *BeppoSAX* observations. While constant-model fits are statistically inconsistent with the *XMM-Newton* p-n, *BeppoSAX* MECS, and *BeppoSAX* LECS light curves, there are no strong, systematic variations about these fits (the poor fit quality appears to be due to stochastic small-amplitude variability only slightly larger than the statistical noise). We can constrain the amplitude of any systematic variability to be $\lesssim 15\%$ for the *XMM-Newton* p-n, $\lesssim 17\%$ for the *BeppoSAX* MECS, and $\lesssim 29\%$ for the *BeppoSAX* LECS. Within the individual observations, no evidence for spectral variability is found upon analysis of hardness ratios (e.g., 2–12 keV to 0.3–2 keV) computed as a function of time. No variability was seen in the *ASCA* data (F99), consistent with our results here.

We have checked for inter-observation spectral variations via joint spectral fitting. A joint spectral analysis of the *XMM-Newton* and *ASCA* data gives a fit with $\chi^2_\nu = 1.04$ (d.o.f. = 1595).⁵ This joint fit is statistically acceptable, indicating that we cannot prove spectral variability between the *ASCA* and *XMM-Newton* observations. If we use the *XMM-Newton* and *BeppoSAX* data, however, we obtain $\chi^2_\nu = 1.20$ (d.o.f. = 1410). This joint fit can be rejected with $> 99.9\%$ confidence, indicating spectral variability. Simultaneous *XMM-Newton* and *BeppoSAX* observations of the Seyfert 1 galaxies NGC 5548 (Pounds et al. 2003) and IC 4329A (Gondoin et al. 2001) have shown that excellent fits can be found in joint spectral analyses, ruling out major cross-calibration errors. The spectral differences between the *XMM-Newton* and *BeppoSAX* data of Mrk 6 are largest below ~ 3 keV where absorption dominates the spectral shape (see Fig. 2), so absorption variability seems a likely explanation. We therefore analyzed the *BeppoSAX* data (MECS, LECS and PDS) individually, which gives best-fit column densities a factor of ~ 2 smaller compared to *XMM-Newton* ($N_{\text{H}}^1 = 4.76^{+0.27}_{-0.25} \times 10^{22} \text{ cm}^{-2}$; $N_{\text{H}}^2 = 1.37^{+0.08}_{-0.07} \times 10^{22} \text{ cm}^{-2}$) and covering fractions which are consistent with our *XMM-Newton* results [$f_c^1 = (54 \pm 1)\%$; $f_c^2 = (95 \pm 1)\%$]. The observed 0.3–2 keV and 2–10 keV *BeppoSAX* fluxes are $1.1 \times 10^{-12} \text{ ergs cm}^{-2} \text{ s}^{-1}$ and $2.4 \times 10^{-11} \text{ ergs cm}^{-2} \text{ s}^{-1}$, respectively. These values are significantly higher than during the *XMM-Newton* observation. The absorption-corrected 2–10 keV flux and luminosity are $3.2 \times 10^{-11} \text{ ergs cm}^{-2} \text{ s}^{-1}$ and $2.1 \times 10^{43} \text{ ergs s}^{-1}$, respectively. The 2–10 keV luminosity of Mrk 6 during the *BeppoSAX* observation was $\sim 60\%$ higher than during the *XMM-Newton* observation.

4. DISCUSSION AND SUMMARY

The analyses above have substantially tightened the constraints upon the X-ray absorption and emission prop-

⁵ The *ASCA* spectra used in this analysis were the same as those presented in F99 (see Tab. 1).

erties of Mrk 6. The *XMM-Newton* spectrum has ~ 7 times as many counts and a wider bandpass than the earlier *ASCA* spectrum, and the 18–120 keV *BeppoSAX* PDS data have provided the first reliable determination of the underlying X-ray continuum shape (a critical quantity for modeling of the X-ray absorption). The absorption measured in the new data can be fit acceptably with the same basic double partial-covering model used to fit the *ASCA* data (F99), providing substantially improved support for the applicability of this model to Mrk 6. The measured column densities are large with N_{H} up to $\sim 10^{23} \text{ cm}^{-2}$, so absorption controls the shape of the X-ray spectrum up to ~ 6 keV. As discussed in §4.2.1 of F99, the absorption seen in X-rays is substantially larger than expected from the optical reddening; the X-ray absorbing material may be dust poor. The small 0.3–1 keV residuals left by the double partial-covering model may be due to $\sim 5 \times 10^{40} \text{ ergs s}^{-1}$ emission from ionized gas in the nucleus or host galaxy. These residuals are consistent with X-ray emission from the Narrow Line Region, similar to that observed in NGC 4151 (Ogle et al. 2000) and the Seyfert 2 galaxies NGC 1068 (Ogle et al. 2003) and Mrk 3 (Sako et al. 2000). The residuals around 0.8–0.9 keV could be Fe L emission, but this spectral complexity is difficult to model due to the limited low-energy photon statistics of the EPIC instruments and the insufficient signal-to-noise ratio of the RGS spectra.

Motivated by recent studies of NGC 4151 (Schurch & Warwick 2002), we also tried fitting the measured X-ray absorption with another physically plausible model consisting of both ionized and neutral columns of gas. This model provides an acceptable fit to the X-ray spectrum above 2 keV, but it leaves substantially larger residuals at lower energies than does the double partial-covering model (visible in the lower panel of Fig. 1). Again these residuals may be plausibly explained by emission from ionized gas in the nucleus or host galaxy.

Three pieces of evidence suggest that, at least at high energies, our X-ray observations have penetrated all the way to the black hole region of Mrk 6: (1) the 18–120 keV continuum shape measured by the *BeppoSAX* PDS is consistent with those of Seyfert 1 galaxies (compare with §3.2 of Malaguti et al. 1999), (2) the relatively small equivalent width of the Fe $K\alpha$ line ($EW = 93_{-20}^{+26} \text{ eV}$) indicates significant dilution of the reflection continuum at 6.4 keV by direct power-law emission from the black hole region, and (3) the relative 2–10 keV, [O III], and far-infrared luminosities are consistent with those of Seyfert 1 galaxies (see §4.1 of F99). Given these results, we can have confidence that

the 2–10 keV ($L_{2-10} = 1.4 \times 10^{43} \text{ ergs s}^{-1}$ from *XMM-Newton*) and 20–100 keV ($L_{20-100} = 3.5 \times 10^{43} \text{ ergs s}^{-1}$ from *BeppoSAX*) luminosities we have found for Mrk 6 represent those of the intrinsic X-ray continuum (rather than just scattered X-ray emission, for example). The X-ray luminosity of Mrk 6 is ~ 5 times the average X-ray luminosity of NGC 4151 ($L_{2-10} \sim 3 \times 10^{42} \text{ ergs s}^{-1}$; $L_{20-100} \sim 1 \times 10^{43} \text{ ergs s}^{-1}$; Yang et al. 2001; Schurch & Warwick 2002; Schurch 2002). Its lower X-ray flux arises only because it is ~ 5.8 times more distant.

Our analyses have also revealed significant X-ray absorption variability during the 1.5 yr between the *BeppoSAX* and *XMM-Newton* observations. In the double partial-covering model, the column densities of both partial covering components drop by a factor of ~ 2 while the covering fractions do not change significantly. If the fitted partial covering in fact indicates that we have both direct, absorbed as well as electron-scattered, unabsorbed views of the nucleus, the observed changes seem physically plausible. The column densities along the direct line of sight could change due to gas motions in the torus atmosphere, while the scattered fraction would not change if scattering occurs on large spatial scales. The mechanism of absorption variability must allow the column density to undergo large fractional changes; such changes could perhaps arise due to bulk rotation of a torus or Poisson fluctuations in a relatively small number of obscuring ‘clouds’ along the line of sight. Our discovery of X-ray absorption variability from Mrk 6 (as well as the observed variability amplitude and timescale) is generally consistent with the absorption variability seen from other absorbed Seyferts (e.g., Risaliti, Elvis, & Nicastro 2002; Schurch & Warwick 2002).

Based on our results, further monitoring of the X-ray absorption variability of Mrk 6 is merited to refine understanding of its amplitude and timescale. Such monitoring could be significantly complemented by coordinated optical spectroscopy, given the known optical line profile variability (see §1). High-quality ultraviolet spectroscopy of Mrk 6 would allow connections to be made between the X-ray absorption and any ultraviolet absorption. The archival *IUE* data on Mrk 6 suggest intrinsic Mg II absorption, but higher quality data are required for a proper study.

We thank L.A. Antonelli, M.C. Eracleous, and N.J. Schurch for helpful discussions. The project was supported by NASA grants NAG5-9940 and LTSA NAG5-8107 and NAG5-13035.

REFERENCES

- Arnaud, K.A. 1996, in ASP Conf. Ser. 101, *Astronomical Data Analysis Software and Systems V*, ed. G.H. Jacoby, & J.Barnes (San Francisco: ASP), 17
- Avni, Y. 1976, *ApJ*, 210, 642
- Branduardi-Raymont, G., Sako, M., Kahn, S.M., Brinkman, A.C., Kaastra, J.S., & Page, M.J. 2001, *A&A*, 365, L140
- Eracleous, M., & Halpern, J.P. 1993, *ApJ*, 409, 584
- Eracleous, M., Halpern, J.P., & Livio, M. 1996, *ApJ*, 459, 89
- Evans, I.N., Tsvetanov, Z., Kriss, G.A., Ford, H.C., Caganoff, S., & Koratkar, A. 1993, *ApJ*, 417, 82
- Jansen, F., Lumb, D., Altieri, B., et al. 2001, *A&A*, 365, L1
- Feldmeier, J.J., Brandt, W.N., Elvis, M., Fabian, A.C., Iwasawa, K., & Mathur, S. 1999, *ApJ*, 510, 167 (F99)
- George, I.M., & Fabian, A.C. 1991, *MNRAS*, 249, 352
- Gondoin, P., Barr, P., Lumb, D., Oosterbroek, T., Orr, A., & Parmar, A.N. 2001, *A&A*, 378, 806
- Kukula, M.J., Holloway, A.J., Pedlar, A., et al. 1996, *MNRAS*, 280, 1283
- Leighly, K.M., Mushotzky, R.F., Yaqoob, T., Kunieda, H., & Edelson, R. 1996, *ApJ*, 469, 147L
- Malaguti, G., et al. 1999, *A&A*, 342, L41
- Malkan, M.A., Gorjian, V., & Tam, R. 1998, *ApJS*, 117, 25
- Matt, G., Brandt, W.N., & Fabian, A.C. 1996, *MNRAS*, 280, 832
- Matt, G., Perola, G.C., Fiore, F., Guainazzi, M., Nicastro, F., & Piro, L. 2000, *A&A*, 363, 863
- Meaburn, J., Whitehead, M.J., & Pedlar, J. 1989, *MNRAS*, 241, 1P
- Nandra, K., George, I.M., Mushotzky, R.F., Turner, T.J., & Yaqoob, T. 1997, *ApJ*, 477, 602

- Ogle, P.M., Marshall, H.L., Lee, J.C., & Canizares, C.R. 2000, *ApJ*, 545, L81
- Ogle, P.M., Brookings, T., Canizares, C.R., Lee, C.J., & Marshall, H.L. 2003, *A&A*, in press, astro-ph/0211406
- Page, M.J., Carrera, F.J., Mittaz, J.P.D., & Mason, K.O. 1999, *MNRAS*, 305, 775
- Page, M.J., Mason, K.O., Carrera, F.J., et al. 2001, *A&A*, 365, L152
- Pounds, K.A., Reeves, J.N., Page, K.L., Edelson, R., Matt, G., & Perola, G.C. 2003, *MNRAS*, submitted, astro-ph/0210288
- Risaliti, G. 2002, *A&A*, 386, 379
- Risaliti, G., Elvis, M., & Nicastro, F. 2002, *ApJ*, 571, 234
- Rosenblatt, E.I., Malkan, M.A., Sargent, W.L.W., & Readhead, A.C.S. 1992, *ApJS*, 81, 59
- Sako, M., Kahn, S.M., Paerels, F., & Liedahl, D.A. 2000, *MNRAS*, 334, 811
- Schurch, N.J., & Warwick, R.S. 2002, *MNRAS*, 334, 811
- Schurch, N.J. 2002, private communication
- Snowden, S.L. 2002, in: *New Visions of the X-ray Universe in the XMM-Newton and Chandra Era*, ESTEC, Noordwijk, The Netherlands, astro-ph/0203311
- Stark, A.A., Gammie, C.F., Wilson, R.W., Bally, J., Linke, R.A., Heiles, C., & Hurwitz, M. 1992, *ApJS*, 79, 77
- Weaver, K.A., Yaqoob, T., Holt, S.S., Mushotzky, R.F., Matsuoka, M., & Yamauchi, M. 1994, *ApJ*, 436, L27
- Yang, Y., Wilson, A.S., & Ferruit, P. 2001, *ApJ*, 563, 124

TABLE 1
X-RAY OBSERVATIONS OF MARKARIAN 6

Observatory	Instr.	Observation ID	Date ^a	Exposure (ks)
ASCA	GIS	75041000	1997-04-07	42.1
ASCA	SIS	75041000	1997-04-07	36.4
<i>BeppoSAX</i>	LECS	51067001	1999-09-14	49.3
<i>BeppoSAX</i>	MECS	51067001	1999-09-14	109.4
<i>BeppoSAX</i>	PDS	51067001	1999-09-14	52.0
<i>XMM-Newton</i>	p-n	0061540101	2001-03-27	31.8
<i>XMM-Newton</i>	MOS 1	0061540101	2001-03-27	30.8
<i>XMM-Newton</i>	MOS 2	0061540101	2001-03-27	30.8
<i>XMM-Newton</i>	RGS 1	0061540101	2001-03-27	46.4
<i>XMM-Newton</i>	RGS 2	0061540101	2001-03-27	37.9

(^a) Start of observation.

TABLE 2
SPECTRAL FITTING PARAMETERS OF MARKARIAN 6

Parameter	Model Description and Data Used ^a			
	(1)	(2)	(3)	(4)
	PL (PDS)	PL+2PC+GA (PDS+p-n+MOS)	RE+2PC+GA (PDS+p-n+MOS)	RE+PI+GA (PDS+p-n+MOS)
Absorption, N_{H} (10^{22} cm ⁻²)	$0.11^{+0.01}_{-0.01}$	$0.11^{+0.01}_{-0.01}$	$0.34^{+0.02}_{-0.01}$
Photon index, Γ	$1.81^{+0.22}_{-0.20}$	1.81 (fixed)
A1 (cts keV ⁻¹ cm ⁻² s ⁻¹)	$9.48^{+0.12}_{-0.10} \times 10^{-2}$	$5.39^{+0.05}_{-0.06} \times 10^{-3}$
Partial covering, N_{H}^1 (10^{22} cm ⁻²)	$10.96^{+0.58}_{-0.42}$	$8.05^{+0.69}_{-0.48}$...
Partial covering, f_c^1 (%)	57^{+1}_{-1}	56^{+2}_{-1}	...
Partial covering, N_{H}^2 (10^{22} cm ⁻²)	$2.46^{+0.07}_{-0.05}$	$2.27^{+0.03}_{-0.08}$...
Partial covering, f_c^2 (%)	93^{+1}_{-1}	91^{+1}_{-1}	...
Photon index, Γ	1.81 (fixed)	1.81 (fixed)
Cutoff energy (keV)	238^{+499}_{-54}	2735^{+383}_{-2368}
Inclination angle, $\cos i$	$0.94^{+0.01}_{-0.25}$	$0.95^{+0.01}_{-0.19}$
Reflection fraction, r	$1.21^{+0.14}_{-0.16}$	$1.33^{+0.21}_{-0.01}$
A2 (cts keV ⁻¹ cm ⁻² s ⁻¹)	$4.68^{+0.02}_{-0.02} \times 10^{-3}$	$4.59^{+0.03}_{-0.06} \times 10^{-3}$
Warm absorption, N_{H} (10^{22} cm ⁻²)	$13.32^{+0.12}_{-0.13}$
Ionization parameter, $\log \xi$	$2.42^{+0.01}_{-0.01}$
Line energy, E (keV)	$6.45^{+0.03}_{-0.04}$	$6.47^{+0.03}_{-0.03}$	$6.45^{+0.04}_{-0.03}$
Line EW (eV)	93^{+26}_{-20}	87^{+20}_{-26}	84^{+19}_{-26}
A3 (cts cm ⁻² s ⁻¹)	$1.85^{+0.60}_{-0.37} \times 10^{-5}$	$1.68^{+0.39}_{-0.53} \times 10^{-5}$	$1.67^{+0.41}_{-0.33} \times 10^{-5}$
$\chi^2/\text{d.o.f.}$ (χ^2_{ν})	3.61/9 (0.40)	824.2/858 (0.96)	812.8/855 (0.95)	937.3/863 (1.09)

Note. — All model fits include Galactic absorption by a column density of $N_{\text{H}} = 6.4 \times 10^{20}$ cm⁻².

(^a)PL: power law; PC: partial covering; GA: Gaussian emission line; PI: photoionized absorption; RE: power law with Compton reflection by neutral material (PEXRAV).

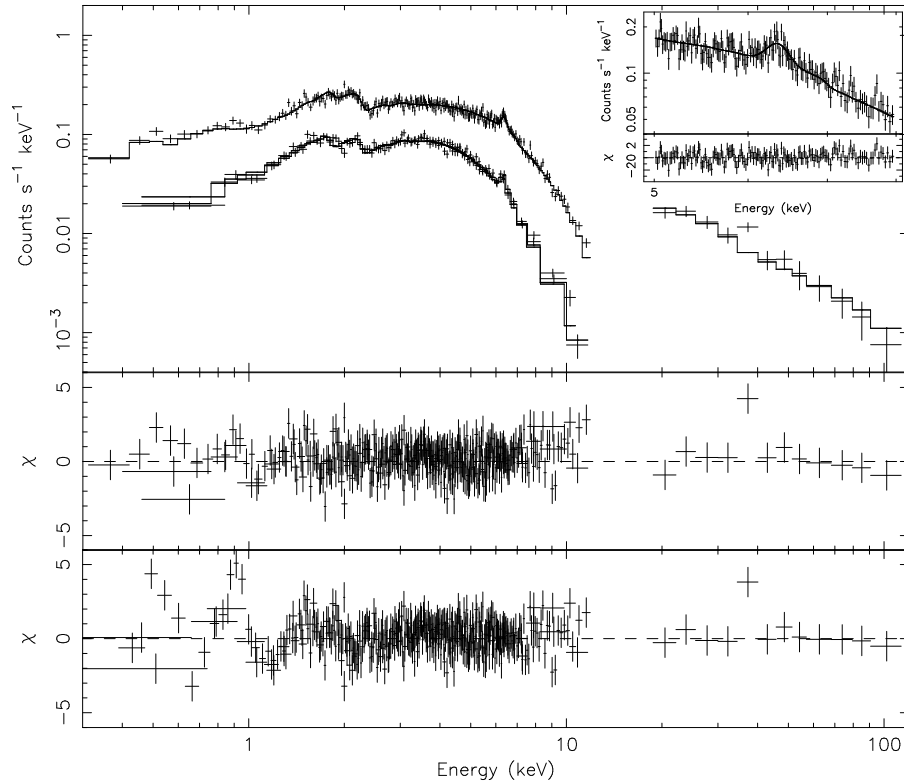


FIG. 1.— *XMM-Newton* EPIC p-n (top), MOS (lower) and *BeppoSAX* PDS (right; > 18 keV) spectra of Mrk 6 in the 0.3–120 keV band. The EPIC counts were binned into energy channels with a signal-to-noise ratio of $S/N > 10$ for plotting purposes. The best-fit double partial-covering model is plotted as the histograms (see model 2 in Tab. 2). The fit residuals from this model are shown in the middle panel (in units of σ). The fit residuals from the partially ionized and neutral absorption model are given in the lower panel (see model 4 in Tab. 2). The positive residual at ~ 38 keV appears to be statistical; we do not find any evidence for a calibration error at this energy, and our results are not materially affected by the exclusion of this data point. The inset shows the (un-binned) 5–8 keV EPIC p-n spectrum around the Fe K α line.

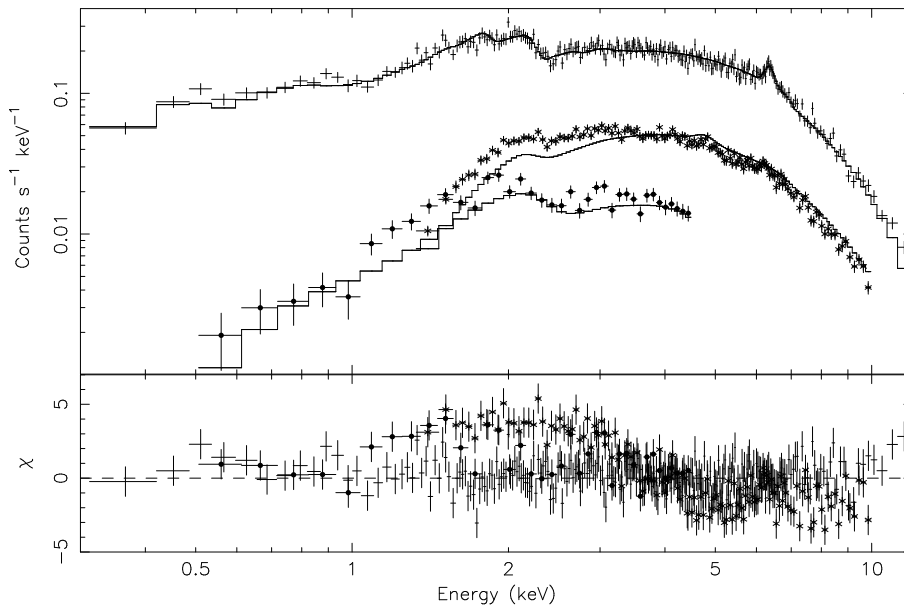


FIG. 2.— *XMM-Newton* EPIC p-n (top; 0.3–12 keV), *BeppoSAX* MECS (middle; 1.3–10 keV) and LECS (lower; 0.5–4.5 keV) spectra of Mrk 6. Counts were binned into energy channels with a signal-to-noise ratio of $S/N > 10$ for plotting purposes. The best-fit double partial-covering model is plotted as the histograms (see model 2 in Tab. 2). The fit residuals are shown in the lower panel (in units of σ). Note the inability to fit the *XMM-Newton* and *BeppoSAX* data simultaneously with the double partial covering model.